



# Machining GLARE fibre metal laminates: a comparative study on drilling effect between conventional and ultrasonic-assisted drilling

Khaled Giasin<sup>1</sup> · Muhammad Atif<sup>2</sup> · Yuan Ma<sup>3,4</sup> · Chulin Jiang<sup>5</sup> · Ugur Koklu<sup>6</sup> · Jos Sinke<sup>7</sup>

Received: 24 June 2022 / Accepted: 7 October 2022  
© The Author(s) 2022

## Abstract

GLARE laminates are multi-layered metal-composite materials created from bonding sheets of metallic alloys with carbon or glass fibre layers. The application of hybrid-conventional machining processes such as ultrasonic-assisted drilling (UAD) is becoming of great interest to the aerospace industry due to its capability in reducing the cutting forces and tool wear which are directly responsible for drilling-induced delamination. There is rich literature on the conventional drilling (CD) of GLARE, but no work reported using UAD process. This study will fill this gap and investigate the UAD of GLARE laminates using an indigenously developed UAD system. The influence of spindle speed and feed rate on thrust force and surface roughness metrics ( $R_a$  and  $R_z$ ) were investigated under CD and UAD regimes. The quality of the borehole and damage mechanisms in the laminate constituents was examined using scanning electron microscopy (SEM). The contribution of the drilling parameters on the measured outputs was further evaluated using the analysis of variance (ANOVA) statistical analysis. It was found that UAD resulted in a significant reduction in thrust force by up to 65% while surface roughness metrics  $R_a$  and  $R_z$  were unaffected by the type of drilling process used. SEM analysis showed irregular and fuzzier surfaces in glass fibre layers in holes machined using UAD due to the longitudinal vibration of the tool.

**Keywords** Ultrasonic-assisted drilling · GLARE · Thrust force · Surface roughness · Scanning electron microscopy

## 1 Introduction

Fibre metal laminates (FMLs) are a group of aerospace multi-materials made from bonding thin metal sheets — usually made from aluminium— and fibre/adhesive layers —usually made from R-glass or S2-glass fibres [1, 2]. Most common FMLs include GLARE® which is made from aluminium and glass-reinforced epoxy, ARALL (FML based on aramid fibres) or CARALL (FML based on carbon fibres) [2, 3]. The alternating nature of FMLs gives it enhanced mechanical properties such as fatigue and crack resistance compared to metallic alloys. Moreover, significant weight reductions are thanks to the lower density of composite layers relative to metals. The thickness of the metallic sheets typically ranges from 0.25 to 0.5 mm, while the laminate thickness can vary between 1 and up to 20 mm [4, 5]. ARALL FMLs were previously tested for use in Boeing 777 cargo floors and liners and on the cargo doors of the C-17 Globemaster III [3]. Currently, composites make up a quarter of the Airbus A380 airframe, with GLARE laminates making up to 3%

✉ Khaled Giasin  
Khaled.giasin@port.ac.uk

<sup>1</sup> Anglesea Building, School of Mechanical and Design Engineering, University of Portsmouth, Anglesea Rd, Portsmouth PO1 3DJ, UK

<sup>2</sup> Beijing Institute of Technology, 5 Zhongguancun St, Haidian District, Beijing 100811, China

<sup>3</sup> State Key Laboratory of Tribology, Department of Mechanical Engineering, Tsinghua University, Beijing 100084, China

<sup>4</sup> Shenzhen Tsingding Technology Co., Ltd, Shenzhen 518101, China

<sup>5</sup> Teesside University, Campus Heart, Southfield Rd, Middlesbrough TS1 3BX, England

<sup>6</sup> Faculty of Engineering, Department of Mechanical Engineering, Karamanoglu Mehmetbey University, Karaman, Turkey

<sup>7</sup> Delft University, Kluyverweg 1, 2629 HS Delft, The Netherlands

[6]. It is estimated that more than 1000 kg weight reduction in Airbus A380 is due to the installation of GLARE laminates instead of monolithic aluminium [7, 8]. The installed GLARE panels in Airbus 380 (about 400 m<sup>2</sup>) showed promising cost savings due to a 25.9% weight reduction [3, 9]. It is estimated that up to 3 million holes are installed in a passenger aircraft, and poor hole quality in aeronautical structures is the main reason for rejection accounting for more than half of all rejected parts [10, 11]. Future projections of air traffic indicate that 33,000 new passenger aircraft will be required annually to meet the rising demands at an estimated value of US\$5.2 trillion in the years 2016–2035 [12]. Therefore, it is important to achieve excellent hole quality to maintain and improve the longevity of aircraft structures [8]. The machinability of FMLs has been the focus of many studies since their introduction. The focus was mainly on conventional drilling (CD) and milling processes as they are the most commonly used machining processes for riveting and assembly operation [2]. Abrasive water jet cutting and laser drilling — which are non-conventional machining processes— were previously used in machining FMLs to evaluate their suitability [13–16]. Early literature on drilling FMLs investigated the influence of drilling parameters, tool coating and geometry, laminate thickness, fibre orientation and cooling strategy on thrust force, torque and a variety of hole metrics. Generally, non-conventional machining of FMLs is not widely reported. Moreover, none of the previous studies investigated UAD process of GLARE laminates.

UAD is hybrid conventional machining that occurs when the cutting tool vibrates (at frequencies around 20,000 Hz and amplitudes of 2–20  $\mu\text{m}$ ) [17, 18]. The excitation of the cutting tool causes it to vibrate either in a torsional or an axial motion [19, 20]. The latter was used in a majority of applications for cutting metals and composites [21, 22]. The purpose of ultrasonic vibrations is to improve chip breakability and reduce friction between the drill and the workpiece [23]. During UAD process, cyclic ultrasonic vibrations reduce the overall contact period of the drill bit with the chips. [18, 24]. UAD can be characterized by the phase shift between the vibrating drill and workpiece such that for vibrational amplitudes at a micro level there is a transition system in which recurring discontinuous contact develops. The recurring discontinuous contact during UAD reduces the cutting forces and tool wear. In addition, the recurring discontinuous contact between the drill and chips means that heat exchange due to thermal conduction becomes less while cooling due to heat convection with the surroundings becomes more [25, 26]. The majority of past research on vibrational and ultrasonic-assisted machining studies reported better tool life, reduced

cutting forces and enhanced hole quality due to the recurring discontinuous contact between the drill and the workpiece [27–30]. There are other types of frequency-assisted machining processes which use different ranges of frequencies and amplitudes such as vibration-assisted machining (VAM) which uses lower frequency range and ultrasonic machining (UM) which uses water-mixed abrasives to erode the workpiece material [17]. UAD is particularly effective for deep-hole drilling where chip clogging is a problem [31]. Previous research reported that UAD tended to improve the surface roughness, burr formations and hole circularity and reduce chip size, tool wear, cutting forces, cutting temperatures and exit delamination (in composites) compared to conventional drilling [32–35]. Nevertheless, some studies reported that UAD process increased the cutting temperatures compared to those generated from CD process using the same cutting parameters and setup [36, 37]. Other studies indicated that the oscillation amplitude and the feed rate affect the thrust force, hole quality parameters and delamination (in composites) compared to spindle speed [18, 38, 39]. It was also reported that UAD reduced cutting forces and produced good hole quality up to a certain level of feed rate and cutting speed beyond which it starts to behave like a CD process [40, 41]. The diminishing influence of ultrasonic vibrations on the cutting action at higher feed rates occurs because of the reduction in maximum value of the effective normal rake angle [18, 36, 41]. Increasing the ultrasonic frequency and its amplitude tended to reduce the cutting forces [39, 42–44]. A limitation from previous studies on vibrational and ultrasonic-assisted machining processes was that most of these systems have been designed for limited range of drill diameter ranging from 3 to 10 mm and using low spindle speeds and feed rates [18]. Previous studies on vibrational and UAD studies show that a frequency of 22 kHz is typical for ultrasonic processes but higher frequencies of up to 40 kHz were also used when machining metals and composites [45–48]

According to the literature, none of the previous studies investigated the machinability of GLARE laminates using UAD process. Therefore, this work aims to fulfil the gap in the literature on this subject and aims to study the UAD of GLARE. The study evaluates the effect of the spindle speed and the feed rate on the developed thrust force and surface roughness parameters ( $R_a$  and  $R_z$ ). Full factorial design (four levels of spindle speed and feed rate) was implemented to establish the relationship between the spindle speed and feed rate —under CD and UAD regimes— on the studied responses. The study also aims to validate whether the UAD process provides any

significant advantage over CD process in terms of the analysed outputs.

## 2 Materials and methods

### 2.1 Workpiece details

A GLARE 2B laminate was used in the current study as shown in Fig. 1a. The metal sheets are Al2024-T3 sheets; the composite layers are S2/FM94 glass fibre. The glass fibre layers are unidirectional and oriented normal to the rolling direction of the metal sheets as shown in Fig. 1a.

Additional details of the laminate are given in Fig. 1b, the thickness of the laminate is 5.96 mm, and the distance between holes centres was 10 mm in X and Y directions. The laminate was manufactured at Delft University of Technology and the FMLC (fibre metal laminates centre of competence). Some of the mechanical properties of S2-Glass fibre prepreg and Al2024-T3 are given in Table 1.

### 2.2 CNC machine setup and drill bit details

The tests were performed on an Ultrasonic-850 machine tool developed by Tsinghua University as shown in Fig. 2. The TSINGDING BT40-ER11-EL ultrasonic tool

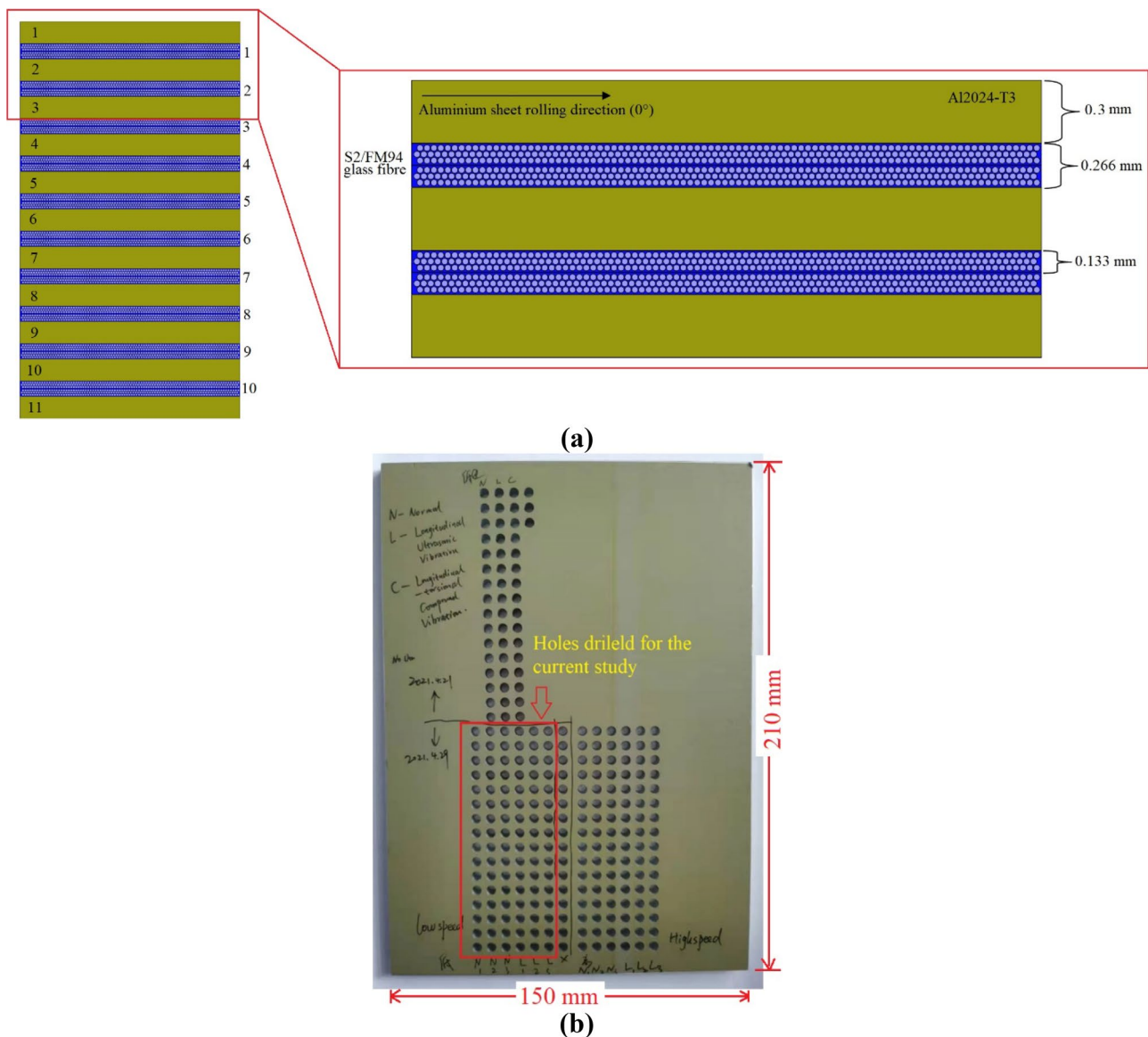
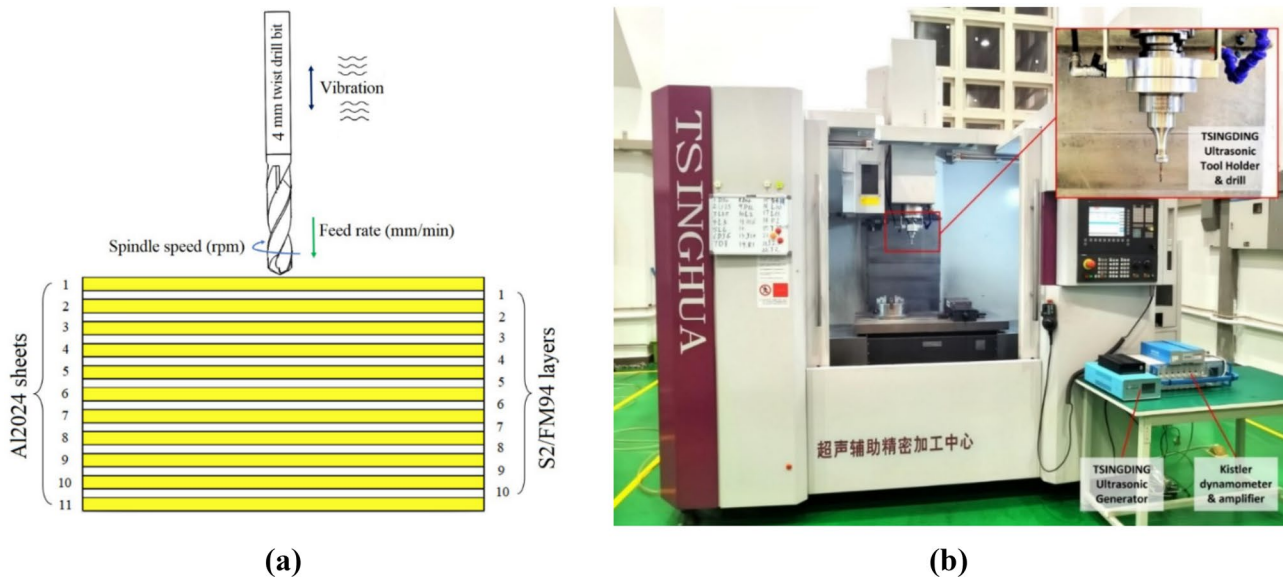


Fig. 1 Schematic representation of a GLARE laminate constituents and b plate after machining tests

**Table 1** Mechanical properties of S2-glass fibre prepreg and Al2024-T3 [49–52]

Mechanical property		UD S2 Glass/FM 94 Epoxy Prepreg $V_F = 60\%$	Al2024-T3	Units
Young's modulus ( $E$ )	L	54–55	72.2	GPa
	T	9.4–9.5	–	
Ultimate tensile strength ( $\sigma_{ult}$ )	L	2640	455	MPa
	T	57	448	
Ultimate strain % ( $\epsilon_{ult}$ )	L	3.5–4.7	19	–
	T	0.6	–	
Shear modulus ( $G$ )	L	5.55	27.6	GPa
	T	3	–	
Poisson's ratio ( $\nu$ )	L	0.33	0.33	–
	T	0.0575	–	
Density ( $\rho$ )	–	1980	2770	kg/m <sup>3</sup>
Thermal expansion coefficient ( $\alpha$ )	L	3.9–6.1	23.4	(1/°C) · 10 <sup>-6</sup>
	T	26.2–55.2	23.4	
Thermal conductivity ( $K$ )	L	1.1–1.4	121	W/m K
	T	0.43–0.53	–	

The symbols  $L$  and  $T$  stand for longitudinal (the rolling direction for the metal) and transverse directions respectively



**Fig. 2** Schematic of UAD process setup of **a** GLARE laminate and cutting tool and **b** thrust force measurement

holder and TSINGDING UMSMT-20–500 intelligent ultrasonic generator were used. The resonant frequency of this ultrasonic tool holder at room temperature and without external loads is 18.7 kHz. During the machining process, the resonant frequency changes with the temperature rise and cutting loads. During this drilling, the resonant frequency ranges from 18.5 to 18.8 kHz. The ultrasonic generator can automatically adjust the electrical output according to the properties of the machining

system, making sure that the system works at its resonant frequency with steady amplitude. The frequency and oscillation amplitudes were measured before the UAD tests to measure the amplitude which the machine cannot provide beforehand. A Keyence laser sensor device was used to measure the vibration amplitude at the tool tip. At 50% duty cycle of UMSMT-20–500 ultrasonic generator, the amplitude is 8  $\mu\text{m}$  (peak to peak amplitude 16  $\mu\text{m}$ ). Four-millimetre-diameter AlCrN-coated carbide

drills were used in the current study. The 4-mm drill size is typical for riveting in aeronautical structures in general and in Airbus A380 in particular. The drills bits have a 140° and 30°-point angle and helix angle, respectively, as they tend to improve chip removal and reduce burr formation.

The tests were conducted using a set of four feed rates and four spindle speeds. The aim is to form a full-factorial design made up of sixteen holes ( $L_{16}$  orthogonal array) as shown in Table 2. The drilling test was repeated twice under the same cutting parameters to confirm the repeatability. Six drills were used, one for each set of holes to avoid any influence arising from the tool wear. ANOVA was employed to examine the significance of the spindle speed, the feed rate and their linear interaction on the measured outputs. The CD and UAD tests were performed without the use of any coolants. The range of

the drilling parameters was determined according to the available literature on machining GLARE and similar aeronautical materials.

### 2.3 Measurement of thrust force

A piezoelectric 6-component KISTLER 9119AA1 (compact multi-component) dynamometer was used to measure the thrust force (up to 4000 N) as shown previously in Fig. 2b. The dynamometer has four 3-component force sensors that can record the compression forces in all directions and translate that to thrust force. DynoWare software version 3.2.5.0, KISTLER data acquisition system type 5697A1 and a charge amplifier type 5080A with 8 channels were used for signal conditioning and data acquisition.

### 2.4 Surface roughness measurement

$R_a$  (the arithmetic average surface roughness) and  $R_z$  (average of the five highest peaks and five lowest valleys) were measured using a Mitutoyo SJ-210 portable surface profilometer. SurfTest SJ USB communication tool version 5.007 software was used to control the roughness tester. The surface roughness parameters were labelled according to ISO 4287 as  $R_a$  (arithmetic mean roughness value) and  $R_z$  (maximum height of profile

**Table 2** Details of parameters used in the UAD study

Machining parameters	Level 1	Level 2	Level 3	Level 4
Spindle speed (rpm)	1000	1500	2000	2500
Feed rate (mm/min)	50	100	150	200
Peak to peak amplitude (µm)	16			
Frequency (kHz)	18.5 to 18.8			

**Fig. 3** Schematic representation of the **a** roughness profiles in GLARE and **b** measurement process of the surface roughness metrics

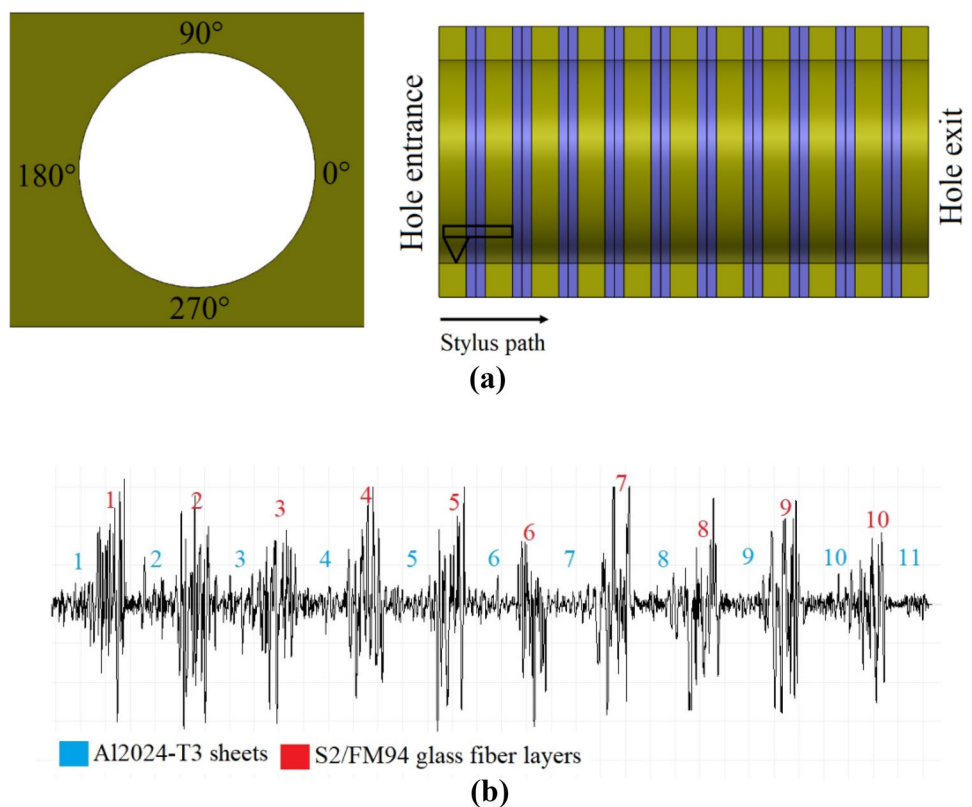
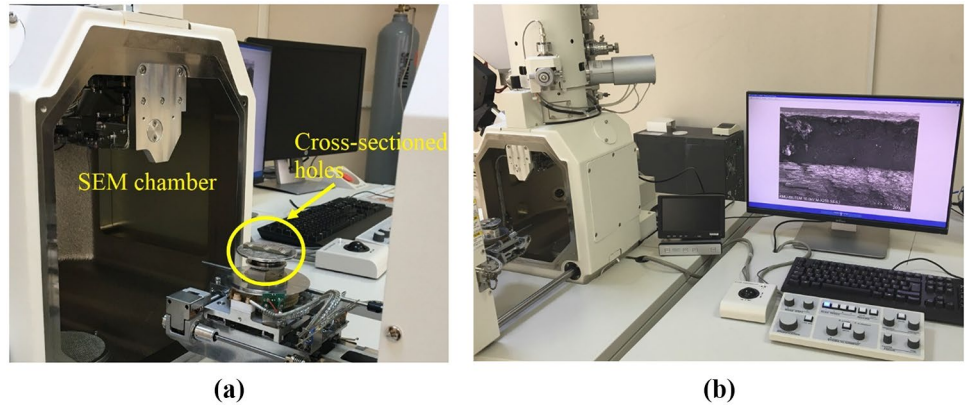


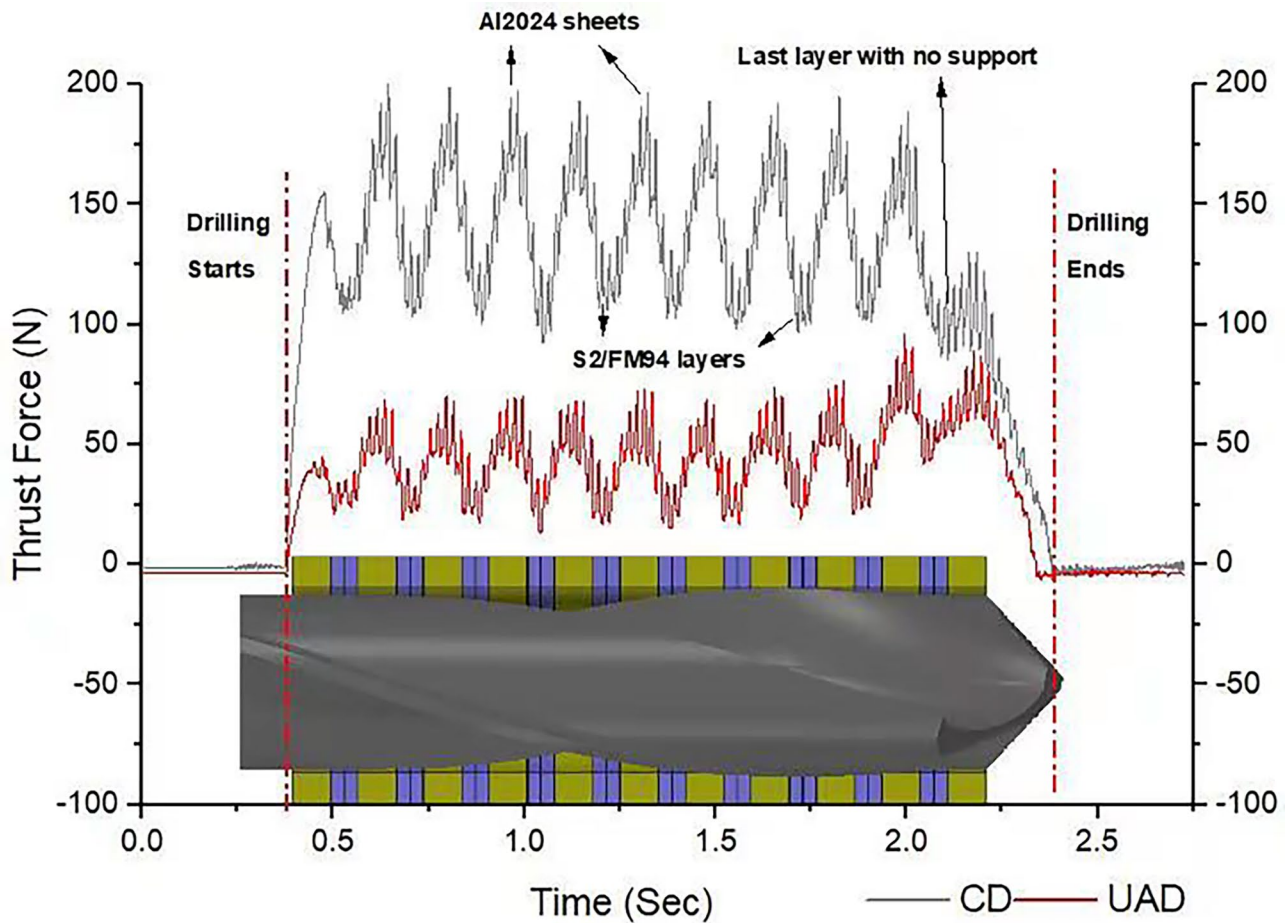
**Fig. 4** Schematic representation of the SEM inspection setup



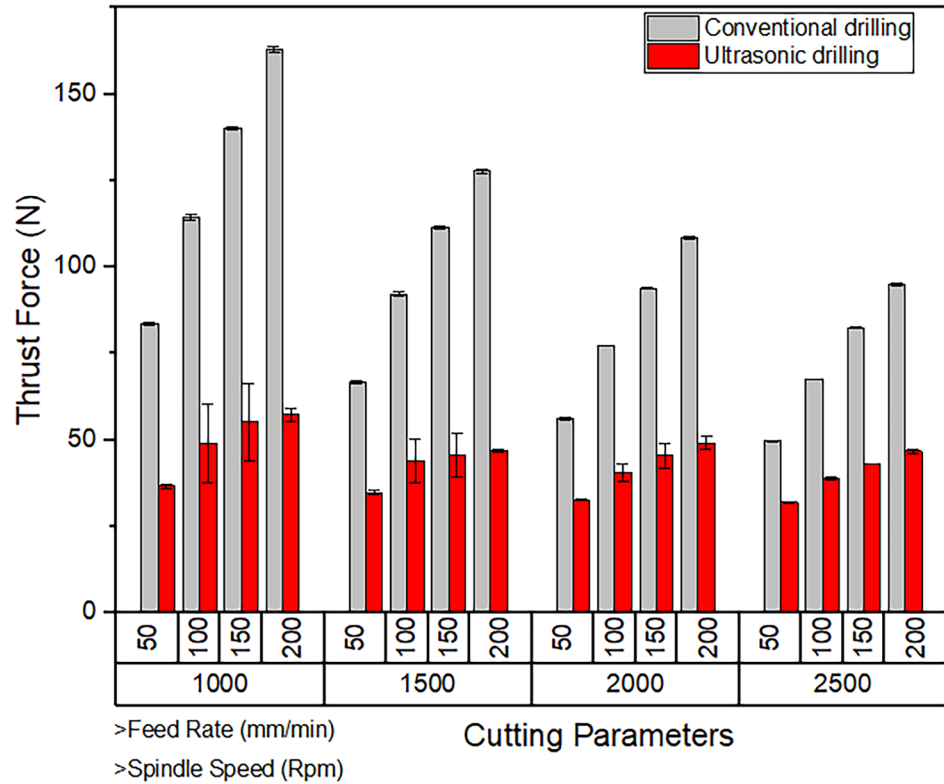
within a sampling length). The roughness metrics were measured four times for each hole at four different locations around its periphery from the hole entry to exit as shown in Fig. 3a, and the mean value of the four readings was reported. The roughness profile of one of the holes drilled in the laminates is shown in Fig. 3b.

### 2.5 Scanning electron microscopy

The holes were cross-sectioned from their centre into two parts using a band saw to observe the condition of the internal surfaces and damage mechanisms in the laminate constituents. An SEM device “Hitachi SU5000”



**Fig. 5** Thrust force profile at  $n= 1000$  rpm and feed rate of  $f= 200$  mm/min

**Fig. 6** Average thrust force under CD and UAD

scanning electron microscope was used to inspect the cross-sectioned holes as shown in Fig. 4. The samples were sputter-coated since the glass fibre layers are non-conductive and can cause difficulties during the scanning process.

### 3 Results and discussion

#### 3.1 Thrust force analysis

The thrust force  $F_z$  was measured from the first interaction of the drill with the top surface of the laminate and until the drill bit exits from the bottom side indicating the end of the drilling process. The reported  $F_z$  values are the average of the three runs. Figure 5 shows the  $F_z$  profile at  $n = 1000$  rpm and  $f = 200$  mm/min for CD and UAD tests. It can be seen that there are three distinct stages which reflect the position of the chisel edge in the laminate at different periods of the drilling process. Initially, the drill and the laminate are not in contact, and therefore, no forces are recorded. Next, the drill becomes in contact as it progresses into the laminate, and a sudden rise in thrust force is observed. It can be seen that the thrust force in the upper and lower aluminium sheets and glass fibre layers is lower than that in the rest of the

laminate layers. This is because the chisel edge is not in full contact with the laminate [53, 54]. The  $F_z$  propagates up to the point where the chisel edges of the drill are in full contact with the laminate, after which a steady maximum force profile is observed [55–57]. Finally,  $F_z$  continuously drops down as the drill disengages from the workpiece indicating the end of the drilling process. From Fig. 5, it can be also seen that the  $F_z$  required for removing material from the aluminium sheets is higher than that required for removing material from the glass fibre layers. Aluminium alloy Al2024 is more dense/compact than the S2 glass fibre layers. In addition, the glass fibre layer has weak resin inside. Moreover, the modulus of elasticity of aluminium alloy Al2024 is much higher than that of S2-glass fibre in secondary and tertiary directions and 31% higher in loading direction [53].

Figure 6 shows the average  $F_z$  obtained from the three runs of the UAD and CD drilling tests for the tested cutting parameters. It can be seen that  $F_z$  increased with the increase of the feed rate and with the decrease of the spindle speed which is in agreement with past studies on CD of GLARE [53, 54, 58, 59]. In CD and UAD, the feed rate was more influential than the spindle speed on the level of  $F_z$ . For example, in CD,  $F_z$  at  $f = 200$  mm/min was 94.9% higher than that at  $f = 50$  mm/min and a constant  $n = 1000$  rpm. Similarly, increasing  $n = 1000$  rpm to  $n = 2500$  rpm at a constant  $f = 50$  mm/min,  $F_z$

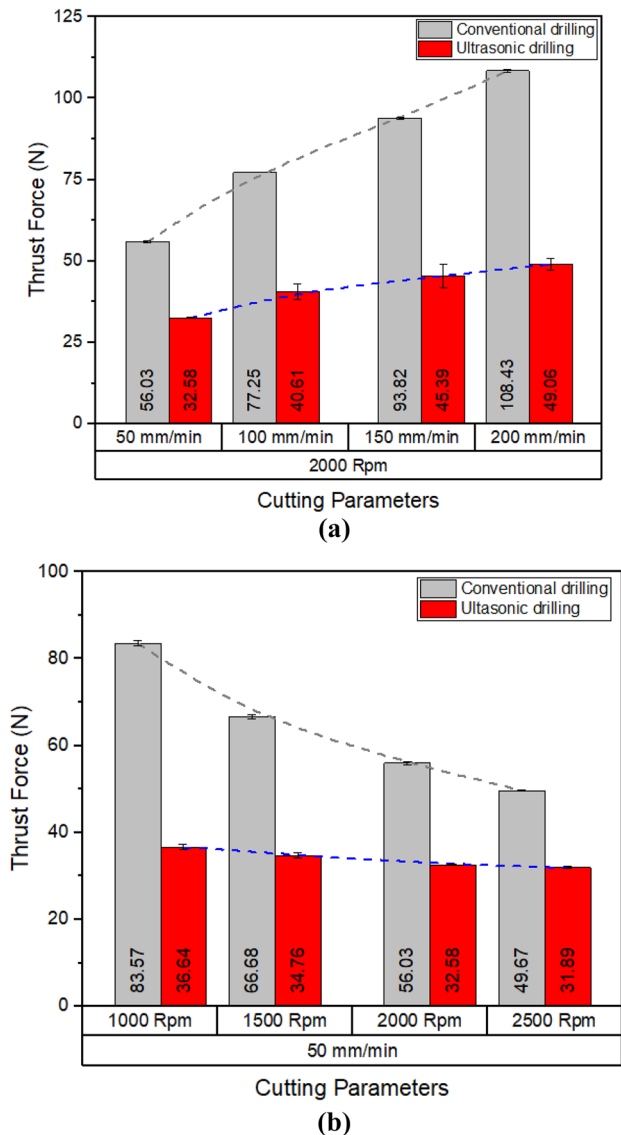


**Fig. 7** Variation of thrust force under UAD and CD with **a** feed rate at 2000 rpm and **b** spindle speed at 50 mm/min

decreased by 40.5%. The same trend is observed in UAD tests; however, the rise in  $F_z$  as the feed rate increased (at a constant spindle speed) is relatively much lower than that observed under CD tests. The same can be said for the decrease in  $F_z$  with the rise in spindle speed (at a constant feed rate). This is mainly attributed to the effect of the vibration on diminishing  $F_z$  which means that drilling time can be significantly reduced without a significant increase of  $F_z$ .

In both the CD and UAD tests,  $F_z$  was minimal at  $f = 50$  mm/min and  $n = 2500$  rpm. Similarly, the highest  $F_z$  was at  $f = 200$  mm/min and  $n = 1000$  rpm. Drilling at feed rates/spindle speeds of 100/1000, 150/1500 and 200/2000

did not cause any significant change in  $F_z$  ( $\sim 5.5\%$ ); this is in disagreement with past studies reported on drilling GLARE [53, 54] which is due to the use of a lower range of drilling parameters in the current study compared to previous studies which used cutting parameters up to  $n = 9000$  rpm and  $= 900$  mm/min, respectively.

The average  $F_z$  generated from UAD tests was significantly lower than those generated from CD tests. For example, under the UAD regime, the average  $F_z$  obtained at  $n = 2500$  rpm and  $f = 200$  mm/min was reduced by 49.22% in comparison to that generated from CD tests. Generally, the average  $F_z$  was reduced by 35.16% and up to 64.20% under UAD tests in comparison to those generated from CD tests using the same drilling parameters. The results indicate that UAD can significantly reduce  $F_z$  which is in agreement with most of the reported studies in the open literature. It was also observed that increasing the feed rate improves the effectiveness of the UAD system as shown in Fig. 7a. The reduction is attributed to the higher separation time between the drill and the laminate, and hence, the friction between the tool and the workpiece decreases [60]. On the contrary, increasing the spindle speed leads to increased contact between the workpiece and the cutting tool—which at a certain point—reduces the UAD effect to behaving like CD process as shown in Fig. 7b. The principle of ultrasonic drilling is to cause the drill to segregate from the workpiece in each vibratory cycle [36]. However, at higher spindle speeds, the contact time at which the drill remains fully engaged with the workpiece increases resembling that found in a CD process [36]. Therefore, as evident from Fig. 7, there is a critical maximum spindle speed and a critical minimum feed rate beyond which the UAD becomes ineffective (i.e., becomes unable to significantly reduce the thrust force in comparison to CD process) which is also influenced by the ultrasonic process parameters (i.e., frequency and amplitude).

When looking at past literature on UAD of different materials, there are no studies reported on FMLs and more specifically on GLARE. However, one can refer to the available literature on UAD of GLARE constituents, i.e., metals (specifically UAD Al2024 and aluminium alloys) and composites (specifically UAD of glass fibre composites) to explain the trends observed in the current study. A significant reduction in thrust force with the increase of the feed rate was also observed in past studies on UAD of Al2024 compared to CD [60]. The study also reported that when using UAD, long continuous chips were produced while broken and fragmented short chips were produced using CD tests. In another study on UAD of Al2024 in a stack made of Ti6Al4V/Al2024-T351 [61], it was found that a vibration frequency of



**Table 3** ANOVA results of the average thrust force

Source	DF	Seq SS	Adj SS	Adj MS	F-value	P-value	Contribution
Model	33	110,406	110,406	3345.6	229.63	0	99.19%
Blocks	2	196	196	97.9	6.72	<b>0.002</b>	0.18%
Linear	7	96,526	96,526	13,789.4	946.43	0	86.72%
Vibration	1	64,855	64,855	64,855.4	4451.32	<b>0</b>	<b>58.27%</b>
Spindle speed	3	12,621	12,621	4206.9	288.74	<b>0</b>	<b>11.34%</b>
Feed rate	3	19,050	19,050	6350	435.83	<b>0</b>	<b>17.11%</b>
2-way interactions	15	13,268	13,268	884.6	60.71	0	11.92%
Vibration*spindle speed	3	6163	6163	2054.2	140.99	<b>0</b>	<b>5.54%</b>
Vibration*feed rate	3	6338	6338	2112.7	145.01	<b>0</b>	<b>5.69%</b>
Spindle speed*feed rate	9	768	768	85.3	5.85	<b>0</b>	<b>0.69%</b>
3-way interactions	9	416	416	46.2	3.17	<b>0.003</b>	0.37%
Vibration*spindle speed*feed rate	9	416	416	46.2	3.17	<b>0.003</b>	<b>0.37%</b>
Error	62	903	903	14.6			0.81%
Total	95	111,309					100.00%

Showing the input parameters with significant contribution on thrust force (highlighted in bold)

20 kHz produced the shortest chip in comparison to CD and UAD other higher frequencies. The studies also reported that the reduction in thrust force as the spindle speed increased was much lower than that when the feed rate was increased [60, 61].

The conclusion which can be drawn from this study is that UAD of GLARE can reduce the thrust force. Also, since the thrust force generated from cutting the aluminium sheets is always greater than that from cutting the glass fibre layers, then it can be suggested that optimisation of the UAD process should be focused on reducing the cutting forces in the metallic sheets in GLARE rather than in the glass fibre layers. The ANOVA analysis is given in Table 3 to highlight the percentage contribution of the machining process (i.e. CD vs UAD), cutting parameters and their linear interaction on the thrust force. The findings show that the vibration had the highest contribution on thrust force with 58.27%, while both drilling parameters also had some effect on the thrust force with a slightly higher contribution for the feed rate with 17.11% followed by the spindle speed with 11.34% similar to previously reported studies [62]. The linear interaction between the two drilling parameters and vibration had a somewhat equal contribution with 5.54–5.69%.

### 3.2 Surface roughness metrics analysis

$R_a$  and  $R_z$  reported here represent the arithmetical mean roughness and the mean roughness depth, respectively, similar to past research on CD of GLARE®. The glass fibre layers had higher roughness than the aluminium sheets due to their fibrous and fuzzy nature after machining as shown previously in Fig. 3b. Figure 8 shows the average measured roughness metrics at

different cutting parameters for UAD and CD tests. For UAD tests,  $R_a$  was between 1.39 and 1.67  $\mu\text{m}$ . For CD tests,  $R_a$  was between 1.42 and 1.78  $\mu\text{m}$ . The highest  $R_a$  occurred at  $n = 2500$  rpm and  $f = 100$  mm/min. The lowest  $R_a$  occurred at  $n = 1500$  rpm and  $f = 50$  mm/min, which indicates that the rise in cutting parameters would increase  $R_a$ . Similarly, for UAD tests,  $R_z$  ranged between 8.09 and 10.45  $\mu\text{m}$ . For CD tests,  $R_z$  ranged between 8.47 and 10.18  $\mu\text{m}$ .

Generally, under CD, the increase in  $R_a$  due to the rise in the feed rate was greater than that due to the rise in the spindle speed. The rise in  $R_a$  with the spindle speed is due to ploughing rather than cutting with chip formation as the un-deformed chip thickness decreases [63]. Comparing  $R_a$  results of UAD against CD, the  $R_a$  in UAD was slightly lower than that in CD at  $n = 1000$  rpm and was higher with the higher spindle speeds of  $n = 1500, 2000,$  and  $2500$  rpm. However, the difference in  $R_a$  between UAD and CD is not significant according to the standard deviations or scatter bands. For example, at  $n = 1000$  rpm,  $R_a$  was 0.03 to 0.14  $\mu\text{m}$  higher than those obtained in CD under the same drilling parameters, while the reduction in  $R_a$  at higher spindle speeds in UAD did not exceed 0.22  $\mu\text{m}$  compared to CD. A firm conclusion can be made that—under the investigated drilling parameters—the UAD process does not provide any significant reduction in surface roughness metric  $R_a$  and  $R_z$  compared to CD.

During UAD of Ti6Al4V alloy, the results showed that at a low feed rate (0.005 mm/tooth), the UAD did not show any significance in terms of surface roughness when compared with conventional drilling, whereas, at a high feed rate (0.015 mm/tooth), the UAD showed considerable improvement at 35 kHz frequency and 8.3  $\mu\text{m}$  amplitude

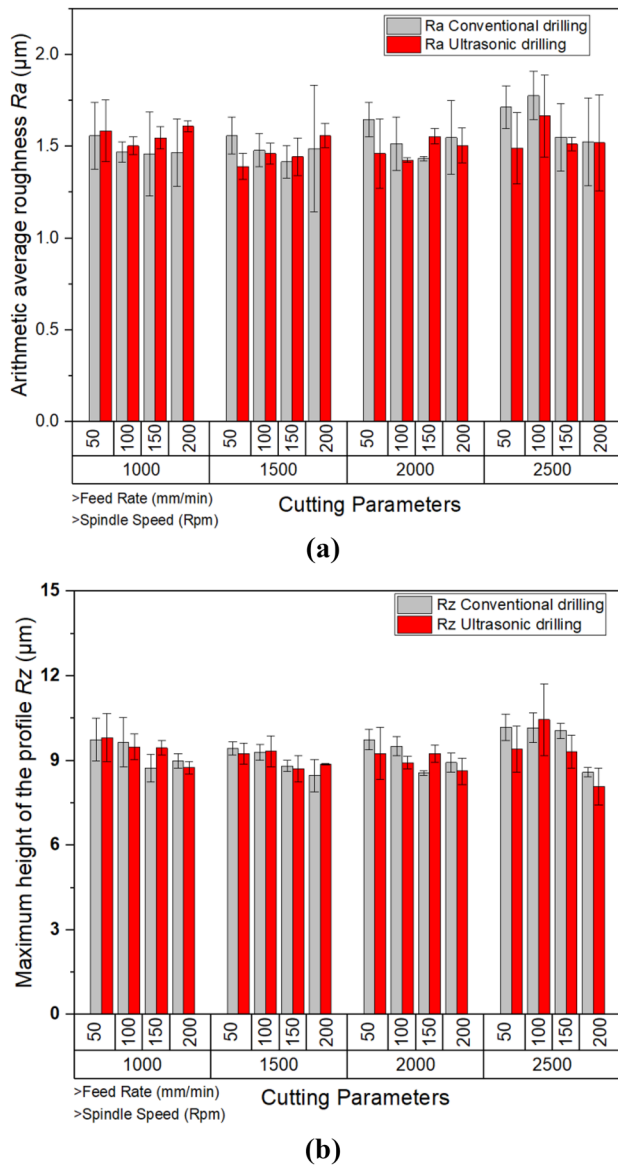


**Fig. 8** Comparison of the average **a**  $R_a$  and **b**  $R_z$  under CD and UAD

[64]. In UAD drilling of composite (epoxy matrix reinforced by glass fibre), the surface roughness showed a significant reduction (more than 50%) using 384 rpm, 1 mm/s, 18.5 kHz frequency, and 0.23  $\mu\text{m}$  amplitude [65]. At lower spindle speed (below 1000 rpm) and low frequency below 338 Hz, the surface roughness did not show any pattern for surface roughness, but with the rise in spindle speed (above 1000 rpm), the surface roughness decreased with the rise in frequency [66]. CFRP composite showed significant improvement in reduction of surface roughness (up to 25%) at low vibration-assisted drilling (LVAD) at frequency 1.5 osc/rev and amplitude of 0.2 mm when compared with conventional drilling [67]. Similarly, the UAD of Al6061 showed that the surface roughness is

mainly affected by the vibration frequency and was less affected by the cutting speed [68]. It showed that with an increase in frequency from 0 to 7.5 Hz, the surface roughness increases and then decreased when it increases from 7.5 to 22.5 Hz. The surface roughness decreased with the rise in spindle speed (535–1525 rpm) but was not significant. In another study during UAD of Al2024, the vibration greatly reduced the surface roughness values [69]. Therefore, it can be said that  $R_a$  is mainly dependent on the number of vibrations per unit length, and as it increases, the surface roughness decreases. Therefore, higher surface roughness reduction in UAD compared to CD can be achieved as high vibration frequency and low spindle speed. The increases in spindle speed also helped in the reduction of the surface roughness due to the reduction in feed rate (mm/rev) which decreases the gap between two consecutive cuts leading to a higher surface finish. The same trend has been reported in UAD of GFRP such that with an increase in cutting speed and decreased feed rate (mm/rev), the surface roughness decreases [70]. A different surface roughness behaviour was observed during UAD of GLARE laminate to that of other isotropic and composite materials. This could be due to the fact that the variation in the mechanical properties of aluminium and glass fibre combined in layers helps in dampening vibration and does not affect the surface roughness compared to other isotropic/composite materials. Literature showed that the surface roughness is mainly affected by the feed rate. The low feed rate helped reduce the surface roughness, but during these experiments, the opposite trend was seen wherein with the rise in the feed rate, the surface roughness decreased which needs more detailed experiments to understand the influence of cutting parameters on the surface finish [71].

The ANOVA results reported in Tables 4 and 5 show that the cutting parameters and use of vibration did not have any contribution to  $R_a$ . Meanwhile, the feed rate had some contribution (26.18%) on  $R_z$  followed by the spindle speed (6.79%), while the use of vibration did not have any impact. There is no acceptable surface roughness for machined GLARE laminates reported in the previous literature or technical documents. However, according to past literature, machined aeronautical structures should have a surface roughness below 3.2 and 1.6  $\mu\text{m}$  in composite and metallic alloys, respectively [54, 63, 72], which means that the range of  $R_a$  in this study from CD and UAD tests is within the bounds of acceptable roughness values for metals and composites.

### 3.3 Scanning electron microscopy analysis

Drilled surfaces, damages caused by the mechanical drilling process and damage types were examined using SEM.

**Table 4** ANOVA results of the average surface roughness  $R_a$ 

Source	DF	Seq SS	Adj SS	Adj MS	F-value	P-value	Contribution
Model	33	0.83672	0.83672	0.025355	0.78	0.782	29.28%
Blocks	2	0.14728	0.14728	0.073639	2.26	0.113	5.15%
Linear	7	0.24307	0.24307	0.034724	1.07	0.396	8.51%
Vibration	1	0.01283	0.01283	0.012829	0.39	0.533	0.45%
Spindle speed	3	0.18102	0.18102	0.06034	1.85	0.147	6.33%
Feed rate	3	0.04922	0.04922	0.016407	0.5	0.681	1.72%
2-way interactions	15	0.40727	0.40727	0.027151	0.83	0.638	14.25%
Vibration*spindle speed	3	0.08989	0.08989	0.029965	0.92	0.437	3.15%
Vibration*feed rate	3	0.13875	0.13875	0.04625	1.42	0.246	4.86%
Spindle speed*feed rate	9	0.17863	0.17863	0.019847	0.61	0.785	6.25%
3-way interactions	9	0.0391	0.0391	0.004345	0.13	0.999	1.37%
Vibration*spindle speed*feed rate	9	0.0391	0.0391	0.004345	0.13	0.999	1.37%
Error	62	2.02115	2.02115	0.032599			70.72%
Total	95	2.85787					100.00%

**Table 5** ANOVA results of the average surface roughness  $R_z$ 

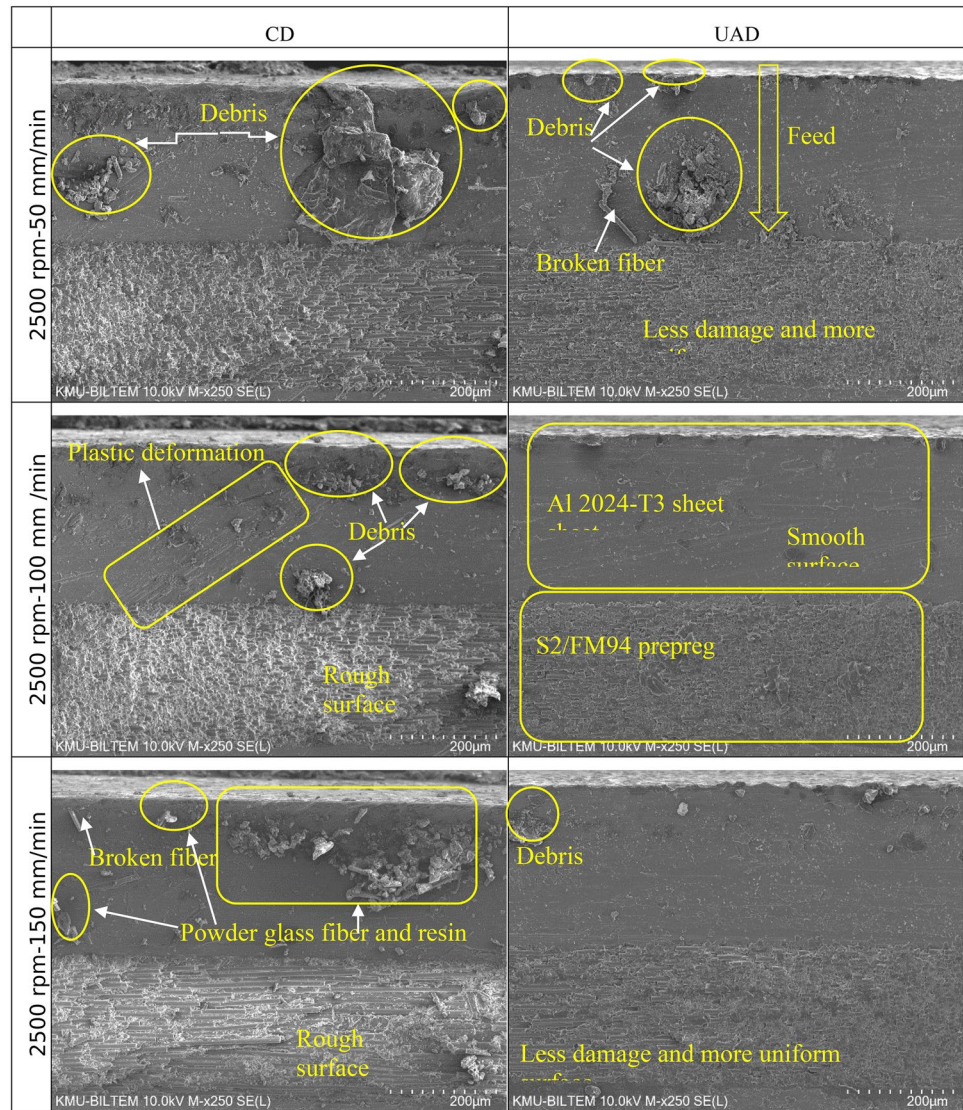
Source	DF	Seq SS	Adj SS	Adj MS	F-value	P-value	Contribution
Model	33	30.339	30.339	0.9194	2.19	0.004	53.85%
Blocks	2	1.2081	1.2081	0.6041	1.44	0.245	2.14%
Linear	7	18.906	18.906	2.7009	6.44	0	33.56%
Vibration	1	0.329	0.329	0.329	0.78	0.379	0.58%
Spindle speed	3	3.8279	3.8279	1.276	3.04	0.035	6.79%
Feed rate	3	14.749	14.749	4.9163	11.72	0	26.18%
2-way interactions	15	7.173	7.173	0.4782	1.14	0.342	12.73%
Vibration*spindle speed	3	1.0286	1.0286	0.3429	0.82	0.489	1.83%
Vibration*feed rate	3	0.7161	0.7161	0.2387	0.57	0.637	1.27%
Spindle speed*feed rate	9	5.4282	5.4282	0.6031	1.44	0.192	9.64%
3-way interactions	9	3.0519	3.0519	0.3391	0.81	0.61	5.42%
Vibration*spindle speed*feed rate	9	3.0519	3.0519	0.3391	0.81	0.61	5.42%
Error	62	25.9993	25.9993	0.4193			46.15%
Total	95	56.3383					100.00%

Figure 9 shows the state of the borehole of metal surfaces under SEM for CD and UAD tests. It demonstrates that the borehole surface of the A12024-T3 sheets, produced by CD tests, was rough including a number of mechanical damages. Plastic deformation, material side flow, debris, broken fibres, powder glass fibre and resin chips were observed. The rise in spindle speed shows increased plastic deformation on the surfaces of the metal sheets in the direction of the spindle speed rotation. Meanwhile, no damage was observed in the transition region from aluminium sheets to glass fibres. CD tests in the aluminium region of the hole, defects can be seen in the borehole surface, including debris, material side flow, plastic deformation, broken fibre, powder glass fibre and resin debris. In the UAD tests, debris and broken fibre

were observed. In general, it can be said that the A12024-T3 region is somewhat smoother in UAD tests, and there is very little debris at the borehole. Ultrasonic impressions were not formed on the borehole surface in UAD tests.

At low spindle speed, the UAD effect is more dominant. The longitudinal vibration with a low feed rate means that the cutting is mostly due to the vertical movement (vibration) of the tool which produces irregular cuts on the fibre layer, which in return results in a fuzzier surface in the glass fibre layers and hence the slightly higher  $R_a$  and  $R_z$  when drilling at  $n = 1000$  rpm as shown previously in Fig. 8. This also increases the deformation in the aluminium sheets, and some chips can be forced or settle on the fuzzy fibre layers. With the increase in the feed rate, the deformation

**Fig. 9** SEM images of the Al 2024-T3 region for CD and UAD tests

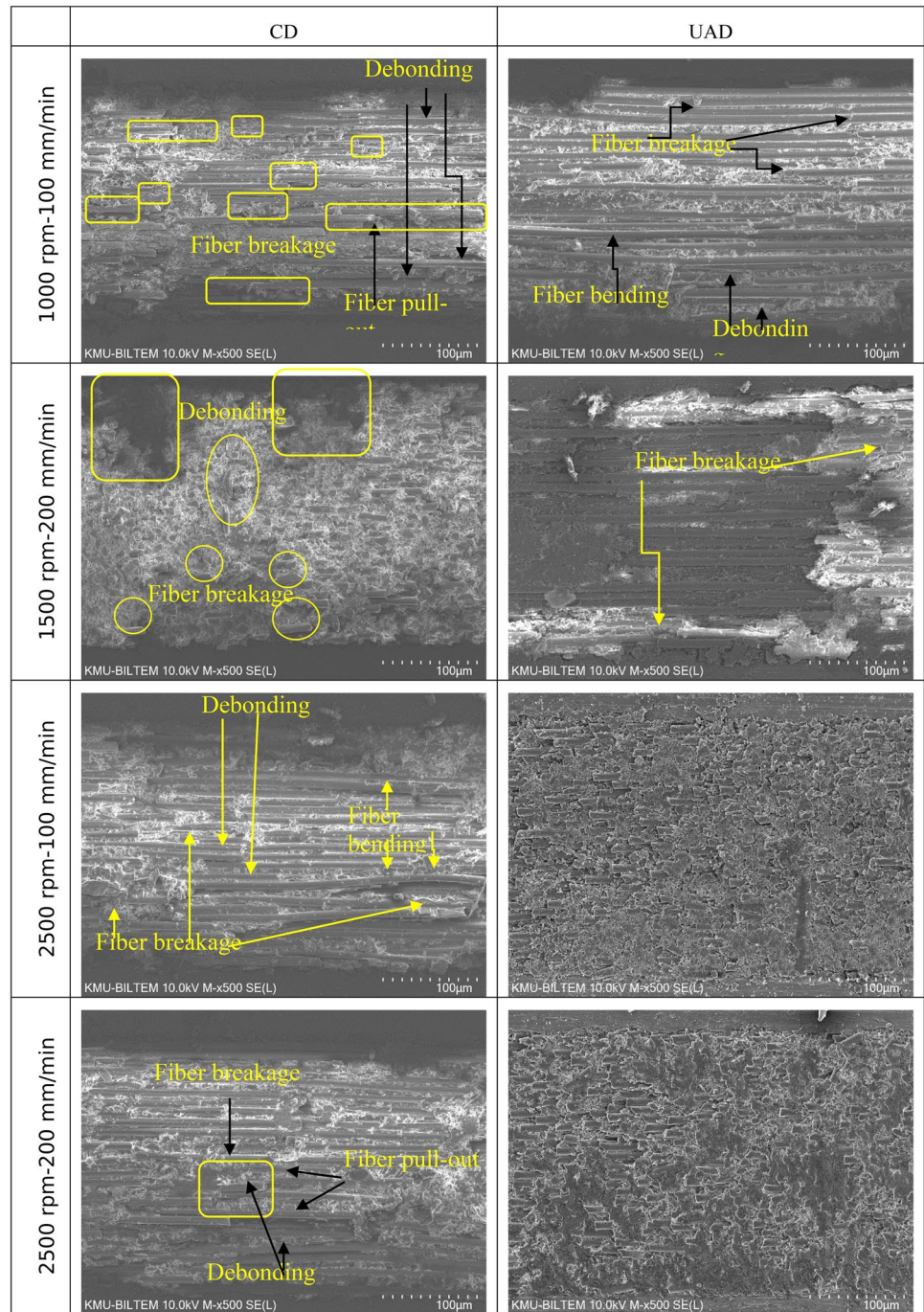


of the aluminium layer is less compared to that observed at low spindle speeds. With the increase in the feed rate, the effect of vibration decreases due to decreases in cutting by the vertical vibration of the tool which results in almost the same quality as that of CD. Increasing the spindle speed while at a constant feed rate reduces the feed per revolution which results in a reduction of chip thickness. When longitudinal vibration is acting on thin chips, it results in the chip breakage and produces serrated chips. At the hole entry, the serrated chips can easily be removed which results in a smoother surface, but at the exit of the hole, the chips are difficult to evacuate. The presence of the chips results in scratches on the hole surface. A small deformation was also observed in the glass fibre layers due to the tool vibration which is not enough to cut/break the longitudinal long exposed fibres.

Damages in the glass fibre zone caused by drilling with CD and UAD are given in Fig. 10. No cracks, separation

or delamination occurred at the glass fibre layers-aluminium sheet interface. Surface damage such as fibre bending, fibre breakage, debonding, fibre pull-out and fibre debonding were extensively observed on the conventional drilled surface. Glass fibre dust particles were scattered all over the borehole surface, and finer dust particles were formed when drilling at low feed rates, especially under CD process. In CD tests performed with a combination of  $n = 1000$  rpm and  $f = 100$  mm/min, extensive fibre breakage occurred on the drilled surfaces. In UAD tests under the same cutting conditions, very little fibre breakage occurred, and a small amount of fibre bending and debonding was observed. In CD experiments, debonding and broken fibre damage occurred intensively in the tests performed with 1500 rpm–200 mm/min. Fibber breakage occurred in UAD experiments. While a smooth surface was obtained in UAD tests at 2500 rpm–100 mm/min and 200 mm/min cutting conditions, significant surface damage occurred in CD tests.

**Fig. 10** SEM images of the AI 2024-T3 region for CD and UAD tests



In the CD tests, debonding, fibre pullout, fibre bending and fibre breakage occurred intensively. Finally, no matrix burning was observed on the hole surface in both methods (CD and UAD) under the selected cutting parameters.

#### 4 Conclusions

The current study investigated the drilling of GLARE fibre metal laminates using ultrasonic-assisted drilling at a

frequency of 18.5–18.85 kHz and amplitude of 16 µm. The aim is to analyse the impact of the ultrasonic vibration on the developed thrust force and surface finish ( $R_a$  and  $R_z$ ). The results of UAD tests were compared against conventional twist drilling tests. The motivation for conducting this study arises from the fact that the influence of UAD process was performed on metals and composites but not on FMLs such as GLARE. According to the experimental results of this study, the following can be concluded:

- The thrust force was reduced by up to 65% under UAD compared to CD process; this is mainly attributed to the continuous variation in the cutting depth of the laminate constituents and periodic separation between the cutting tool and the laminate.
- To reduce the thrust force, a low feed rate and a high spindle speed are recommended.
- The surface roughness  $R_a$  and  $R_z$  ranged between 1.4 and 1.8  $\mu\text{m}$  and between 8 and 10.5  $\mu\text{m}$ , respectively, under CD and UAD regimes.
- The surface roughness ( $R_a$  and  $R_z$ ) results under CD and UAD regimes were similar, which means that the use of vibration during drilling of GLARE laminates will not yield any significant improvement in the laminate surface finish. This is mainly attributed to the way GLARE constituents are stacked alternatively in the form of thin sheets/layers.
- There are other factors which can affect the UAD process other than the feed rate and spindle speed such as chip removal mechanisms, frequency, amplitude, duty cycle and phase shift all of which require systematic experiments to evaluate their impact on the drilling process. These factors will be investigated in future studies.

**Data availability** The data used in this work can be requested by contacting the authors.

**Code availability** Not applicable.

## Declarations

**Ethics approval** Not applicable.

**Consent to participate** Not applicable.

**Consent for publication** Not applicable.

**Competing interests** The authors declare no competing interests.

**Open Access** This article is licensed under a Creative Commons Attribution 4.0 International License, which permits use, sharing, adaptation, distribution and reproduction in any medium or format, as long as you give appropriate credit to the original author(s) and the source, provide a link to the Creative Commons licence, and indicate if changes were made. The images or other third party material in this article are included in the article's Creative Commons licence, unless indicated otherwise in a credit line to the material. If material is not included in the article's Creative Commons licence and your intended use is not permitted by statutory regulation or exceeds the permitted use, you will need to obtain permission directly from the copyright holder. To view a copy of this licence, visit <http://creativecommons.org/licenses/by/4.0/>.

## References

1. Vlot A, Vogelesang L, De Vries T (1999) Towards application of fibre metal laminates in large aircraft. *Aircr Eng Aerosp Technol* 71(6):558–570
2. Vlot A, Gunnink JW (2001) Fibre metal laminates: an introduction. Springer. <https://doi.org/10.1007/978-94-010-0995-9>
3. Vlot A (2001) Glare: history of the development of a new aircraft material, 1st edn. Springer Science & Business Media, p 228. <https://doi.org/10.1007/0-306-48398-X>
4. De Graaf R, Meijer J (2000) Laser cutting of metal laminates: analysis and experimental validation. *J Mater Process Technol* 103(1):23–28
5. Geert HJJ, Roebroeks PAH, Kroon EJ, Heinimann MB (2007) The development of central. In: Benedictus JSR, Alderliesten RC, Homan JJ (eds) First International Conference on Damage Tolerance of Aircraft Structures. TU Delft, The Netherlands
6. Graham-Cumming J (2009) The Geek Atlas: 128 places where science and technology come alive. O'Reilly Media, Inc, p 545
7. Black S (2017) Fiber-metal laminates in the spotlight. Cited 14 Jan 2019
8. Giasin K (2018) The effect of drilling parameters, cooling technology, and fiber orientation on hole perpendicularity error in fiber metal laminates. *Int J Adv Manuf Technol*. <https://doi.org/10.1007/s00170-018-2241-1>
9. Chawla KK (2012) Composite materials: science and engineering. Springer Science & Business Media. <https://doi.org/10.1007/978-0-387-74365-3>
10. Mouritz A (2012) Introduction to aerospace materials. Elsevier, Woodhead Publishing, p 640
11. Hocheng H (2012) Machining technology for composite materials: principles and practice. Woodhead Pub, Cambridge
12. Airbus, Mapping Demand 2016–2035 (2016) Global market forecast. Available from <http://www.airbus.com/company/market/global-market-forecast-2016-2035/>
13. Welschen R, Hoogstrate A, van Lutervelt C, Kals H, Paul S (1997) High pressure abrasive water jet machining of metal polymer laminates. In Proceedings of 17th All India Manufacturing Technology: Design and Research Conference. Allied Publishers
14. Paul S, Hoogstrate A, Van Praag R (2002) Abrasive water jet machining of glass fibre metal laminates. *Proc Inst Mech Eng B J Eng Manuf* 216(11):1459–1469
15. Ramulu M, Pahuja R, Hashish M, Isvilonanda V (2015) Abrasive waterjet machining effects on kerf quality in thin fiber metal laminate. In 2015 WJTA-IMCA Conference and Expo. WJTA-IMCA®, New Orleans
16. Ramulu M, Isvilonanda V, Pahuja R, Hashish M (2016) Experimental investigation of abrasive waterjet machining of titanium graphite laminates. *Int J Autom Technol* 10(3):392–400. <https://doi.org/10.20965/ijat.2016.p0392>
17. Moghaddas M, Short M, Wiley N, Yi A, Graff K (2018) Performance of an ultrasonic-assisted drilling module. *Int J Adv Manuf Technol* 94(9–12):3019–3028. <https://doi.org/10.1007/s00170-017-0495-7>
18. Gupta A (2016) Study of cutting speed on ultrasonic assisted drilling of carbon fibre reinforced plastics. University of Warwick. Available from <http://wrap.warwick.ac.uk/81993/>
19. Astashev VK, Babitsky VI (2007) Ultrasonic processes and machines: dynamics, control and applications. Springer Science & Business Media, p 332. <https://doi.org/10.1007/978-3-540-72061-4>
20. Neugebauer R, Stoll A (2004) Ultrasonic application in drilling. *J Mater Process Technol* 149(1–3):633–639. <https://doi.org/10.1016/j.jmatprotec.2003.10.062>
21. Azarhoushang B, Akbari J (2007) Ultrasonic-assisted drilling of Inconel 738-LC. *Int J Mach Tools Manuf* 47(7–8):1027–1033. <https://doi.org/10.1016/j.ijmachtools.2006.10.007>
22. Vakili Azghandi B, Razfar MR (2011) An experimental study on the effects of ultrasonic assisted drilling on chip characteristics and tool life. *Advanced Materials Research*. *Trans Tech Publ*. <https://doi.org/10.4028/www.scientific.net/AMR.325.351>

23. Astakhov VP, Patel S, Woon KS (2018) Drilling technology: fundamentals and recent advances. *Adv Mech Eng* 3:191. <https://doi.org/10.1515/9783110481204>. Walter de Gruyter GmbH & Co KG
24. Patil S, Joshi S, Tewari A (n.d.) Microstructural analysis of ultrasonic vibration assisted turning of Ti alloy Ti-6Al-4V. In: Proceedings of the 8th International Conference on MicroManufacturing. Available from <https://minds.wisconsin.edu/handle/1793/70109?show=full>
25. Patil S, Joshi S, Tewari A, Joshi SS (2014) Modelling and simulation of effect of ultrasonic vibrations on machining of Ti6Al4V. *Ultrasonics* 54(2):694–705. <https://doi.org/10.1016/j.ultras.2013.09.010>
26. Maurotto A, Roy A, Babitsky VI, Silberschmidt VV (2012) Analysis of machinability of Ti-and Ni-based alloys. *Solid State Phenomena*. Trans Tech Publ. <https://doi.org/10.4028/www.scientific.net/SSP.188.330>
27. Baghlani V, Mehbudi P, Akbari J, Sohrabi M (2013) Ultrasonic assisted deep drilling of Inconel 738LC superalloy. *Procedia CIRP* 6:571–576. <https://doi.org/10.1016/j.procir.2013.03.096>
28. Liao Y, Chen Y, Lin H (2007) Feasibility study of the ultrasonic vibration assisted drilling of Inconel superalloy. *Int J Mach Tools Manuf* 47(12–13):1988–1996. <https://doi.org/10.1016/j.ijmactools.2007.02.001>
29. Amini S, Soleimani M, Paktinat H, Lotfi M (2017) Effect of longitudinal–torsional vibration in ultrasonic-assisted drilling. *Mater Manuf Processes* 32(6):616–622. <https://doi.org/10.1080/10426914.2016.1198027>
30. Nath C, Rahman M (2008) Effect of machining parameters in ultrasonic vibration cutting. *Int J Mach Tools Manuf* 48(9):965–974. <https://doi.org/10.1016/j.ijmactools.2008.01.013>
31. Stephenson DA, Agapiou JS (2016) Metal cutting theory and practice. CRC Press, p 969. <https://doi.org/10.1201/9781315373119>
32. Chang SS, Bone GM (2005) Burr size reduction in drilling by ultrasonic assistance. *Robot Comput Integr Manuf* 21(4–5):442–450. <https://doi.org/10.1016/j.rcim.2004.11.005>
33. Chang SS, Bone GM (2009) Thrust force model for vibration-assisted drilling of aluminum 6061–T6. *Int J Mach Tools Manuf* 49(14):1070–1076. <https://doi.org/10.1016/j.ijmactools.2009.07.011>
34. Chern G-L, Lee H-J (2006) Using workpiece vibration cutting for micro-drilling. *Int J Adv Manuf Technol* 27(7–8):688–692. <https://doi.org/10.1007/s00170-004-2255-8>
35. Thomas P, Babitsky V (2007) Experiments and simulations on ultrasonically assisted drilling. *J Sound Vib* 308(3–5):815–830. <https://doi.org/10.1016/j.jsv.2007.03.081>
36. Makhdum F, Phadnis VA, Roy A, Silberschmidt VV (2014) Effect of ultrasonically-assisted drilling on carbon-fibre-reinforced plastics. *J Sound Vib* 333(23):5939–5952. <https://doi.org/10.1016/j.jsv.2014.05.042>
37. Pujana J, Rivero A, Celaya A, De Lacalle LL (2009) Analysis of ultrasonic-assisted drilling of Ti6Al4V. *Int J Mach Tools Manuf* 49(6):500–508. <https://doi.org/10.1016/j.ijmactools.2008.12.014>
38. Mehbudi P, Baghlani V, Akbari J, Bushroa A, Mardi N (2013) Applying ultrasonic vibration to decrease drilling-induced delamination in GFRP laminates. *Procedia Cirp* 6:577–582. <https://doi.org/10.1016/j.procir.2013.03.097>
39. Li Z, Zhang D, Qin W, Geng D (2016) Removal analyses of chip and rod in rotary ultrasonic-assisted drilling of carbon fiber-reinforced plastics using core drill. *J Reinf Plast Compos* 35(15):1173–1190. <https://doi.org/10.1177/0731684416644510>
40. Vedvik N (2015) Assessment of ultrasonic assisted drilling. NTNU:85. Available from [https://ntnuopen.ntnu.no/ntnu-xmlui/bitstream/handle/11250/2351193/13283\\_FULLTEXT.pdf?sequence=1&isAllowed=y](https://ntnuopen.ntnu.no/ntnu-xmlui/bitstream/handle/11250/2351193/13283_FULLTEXT.pdf?sequence=1&isAllowed=y)
41. Onawumi PY, Roy A, Silberschmidt VV, Merson E (2018) Ultrasonically assisted drilling of aerospace CFRP/Ti stacks. *Procedia CIRP* 77:383–386. <https://doi.org/10.1016/j.procir.2018.09.041>
42. Alam K, Silberschmidt VV (2014) Analysis of temperature in conventional and ultrasonically-assisted drilling of cortical bone with infrared thermography. *Technol Health Care* 22(2):243–252. <https://doi.org/10.3233/THC-140813>
43. Alam K, Mitrofanov A, Silberschmidt VV (2011) Experimental investigations of forces and torque in conventional and ultrasonically-assisted drilling of cortical bone. *Med Eng Phys* 33(2):234–239. <https://doi.org/10.1016/j.medengphy.2010.10.003>
44. Alam K, Hassan E, Bahadur I (2015) Experimental measurements of temperatures in ultrasonically assisted drilling of cortical bone. *Biotechnol Biotechnol Equip* 29(4):753–757. <https://doi.org/10.1080/13102818.2015.1034176>
45. Kadivar M, Akbari J, Yousefi R, Rahi A, Nick MG (2014) Investigating the effects of vibration method on ultrasonic-assisted drilling of Al/SiCp metal matrix composites. *Robot Comput Integr Manuf* 30(3):344–350. <https://doi.org/10.1016/j.rcim.2013.10.001>
46. Phadnis VA, Roy A, Silberschmidt VV (2013) A finite element model of ultrasonically assisted drilling in carbon/epoxy composites. *Procedia Cirp* 8:141–146. <https://doi.org/10.1016/j.procir.2013.06.079>
47. Gupta A, Ascroft H, Barnes S (2016) Effect of chisel edge in ultrasonic assisted drilling of carbon fibre reinforced plastics (CFRP). *Procedia CIRP* 46:619–622. <https://doi.org/10.1016/j.procir.2016.04.026>
48. Li Z, Zhang D, Jiang X, Qin W, Geng D (2017) Study on rotary ultrasonic-assisted drilling of titanium alloys (Ti6Al4V) using 8-facet drill under no cooling condition. *Int J Adv Manuf Technol* 90(9–12):3249–3264. <https://doi.org/10.1007/s00170-016-9593-1>
49. De Vries TJ (2001) Blunt and sharp notch behaviour of Glare laminates. In: Aerospace Engineering. Delft University Press, p 432. Available from <https://repository.tudelft.nl/islandora/object/uuid%3Abd3b2294-e095-407d-bb8d-1c66f6651ae8>
50. Mohit G, Frank A, Michael F, Galib A (2011) Predicting bearing strength of fiber metal laminates via progressive failure analysis. In 52nd AIAA/ASME/ASCE/AHS/ASC Structures, Structural Dynamics and Materials Conference. American Institute of Aeronautics and Astronautics. <https://doi.org/10.2514/6.2011-2055>
51. Yaghoubi AS, Liaw B (2013) Damage assessments of ballistic impact behaviors of GLARE 5 (3/2) beams with various stacking sequences. In: Dynamic behavior of materials, vol 1. Springer, pp 503–512. [https://doi.org/10.1007/978-1-4614-4238-7\\_65](https://doi.org/10.1007/978-1-4614-4238-7_65)
52. Hagenbeek M (2005) Characterisation of fibre metal laminates under thermomechanical loadings. TU Delft, Delft University of Technology. Available from <https://repository.tudelft.nl/islandora/object/uuid%3A2c91c8bd-b0a4-4c3b-86ee-f5ad8f1ea24e>
53. Giasin K, Ayvar-Soberanis S, Hodzic A (2015) An experimental study on drilling of unidirectional GLARE fibre metal laminates. *Compos Struct* 133:794–808. <https://doi.org/10.1016/j.compstruct.2015.08.007>
54. Giasin K (2017) Machining fibre metal laminates and Al2024-T3 aluminium alloy. University of Sheffield, Available from: <http://etheses.whiterose.ac.uk/16061/>
55. Bhudwannachai P (2014) Performance evaluation and analysis of the use of CO2 cooling for conventional drilling of carbon fibre reinforced plastics. University of Warwick. Available from <http://wrap.warwick.ac.uk/66880/>
56. Sheikh-Ahma JY (2009) Machining of polymer composites. Springer, p 315. <https://doi.org/10.1007/978-0-387-68619-6>
57. Davim JP (2008) Machining: fundamentals and recent advances. Springer Science & Business Media, p 362. <https://doi.org/10.1007/978-1-84800-213-5>
58. Giasin K, Ayvar-Soberanis S, Hodzic A (2016) The effects of minimum quantity lubrication and cryogenic liquid nitrogen

- cooling on drilled hole quality in GLARE fibre metal laminates. *Mater Des* 89:996–1006
59. Giasin K, Ayvar-Soberanis S, French T, Phadnis V (2016) 3D finite element modelling of cutting forces in drilling fibre metal laminates and experimental hole quality analysis. *Appl Compos Mater*:1–25. <https://doi.org/10.1007/s10443-016-9517-0>
  60. Barani A, Amini S, Paktinat H, Tehrani AF (2014) Built-up edge investigation in vibration drilling of Al2024-T6. *Ultrasonics* 54(5):1300–1310. <https://doi.org/10.1016/j.ultras.2014.01.003>
  61. Wei L, Wang D (2019) Comparative study on drilling effect between conventional drilling and ultrasonic-assisted drilling of Ti-6Al-4V/Al2024-T351 laminated material. *Int J Adv Manuf Technol*:103. <https://doi.org/10.1007/s00170-019-03507-6>
  62. Zhu X-X, Wang W-H, Jiang R-S, Xiong Y-F, Liu X-F (2022) Thrust force model for ultrasonic-assisted micro drilling of DD6 superalloy. *Adv Manuf*. <https://doi.org/10.1007/s40436-021-00381-y>
  63. Giasin K, Gorey G, Byrne C, Sinke J, Brousseau E (2019) Effect of machining parameters and cutting tool coating on hole quality in dry drilling of fibre metal laminates. *Compos Struct*. <https://doi.org/10.1016/j.compstruct.2019.01.023>
  64. Sorgato M, Bertolini R, Ghiotti A, Bruschi S (2021) Tool wear analysis in high-frequency vibration-assisted drilling of additive manufactured Ti6Al4V alloy. *Wear* 477:203814. <https://doi.org/10.1016/j.wear.2021.203814>
  65. Aoki S, Hirai S, Nishimura T (2005) Prevention from delamination of composite material during drilling using ultrasonic vibration. *Key Engineering Materials*. Trans Tech Publ. <https://doi.org/10.4028/www.scientific.net/KEM.291-292.465>
  66. Aoki S, Nishimura T (2004) Prevention of delamination during drilling of composite material using vibration. *Key Engineering Materials*. Trans Tech Publ. <https://doi.org/10.4028/www.scientific.net/KEM.261-263.381>
  67. Xu J, Li C, Chen M, Ren F (2019) A comparison between vibration assisted and conventional drilling of CFRP/Ti6Al4V stacks. *J Mater Manuf Process* 34(10):1182–1193. <https://doi.org/10.1080/10426914.2019.1615085>
  68. Yazar E, Karabay S (2020) Investigation of the effects of ultrasonic assisted drilling on tool wear and optimization of drilling parameters. *CIRP J Manuf Sci Technol* 31:265–280
  69. Barani A, Amini S, Paktinat H, Tehrani AF (2014) Built-up edge investigation in vibration drilling of Al2024-T6. *Ultrasonics* 54(5):1300–1310
  70. Palanikumar KJM (2010) Modeling and analysis of delamination factor and surface roughness in drilling GFRP composites. *Mater Manuf Process* 25(10):1059–1067
  71. Raj AM, Das SL, Palanikumar K (2013) Influence of drill geometry on surface roughness in drilling of Al/SiC/Gr hybrid metal matrix composite. *Indian J Sci Technol* 6(7):5002–5007
  72. Coromant S (2010) Machining carbon fibre materials, in Sandvik coromant user's guide - composite solutions, Available from: <http://www.sandvik.coromant.com/SiteCollectionDocuments/downloads/global/technical%20guides/en-gb/C-2920-30.pdf>

**Publisher's note** Springer Nature remains neutral with regard to jurisdictional claims in published maps and institutional affiliations.